Suppl. Table 1. Initial biogeochemical conditions for the Fe-NO, Fe-NEW, and Fe-REG treatments.

	Fe-NO	**Fe-NEW**	**Fe-REG**
Ammonium (μM)	1.22 ± 0.16	0.72 ± 0.24	1.03 ± 0.34
Nitrate (μM)	22.36 ± 0.76	23.26 ± 0.17	23.20 ± 0.03
Nitrite (μM)	0.35 ± 0.07	0.44 ± 0.01	0.45 ± 0.01
Phosphate (μM)	1.62 ± 0.06	1.68 ± 0.01	1.69 ± 0.01
Silicate (μM)	3.16 ± 0.08	5.43 ± 0.01	6.07 ± 0.07
Dissolved iron (nM)	0.11 ± 0.01	0.16 ± 0.04	0.26 ± 0.02
Chlorophyll-a (μg L^{-1})	0.154 ± 0.016	0.132 ± 0.015	0.132 ± 0.003
F_v/F_m	0.52 ± 0.05	0.50 ± 0.05	0.44 ± 0.04

Suppl. Table 2. Iron and carbon uptake rates for the different components of the in-eddy phytoplankton community (from companion paper Ellwood et al. 2020).

	0.2-2-μm [a,b]	2-20-μm [a,b]	>20-μm [a,b]
Fe uptake (pmol L^{-1} d^{-1})	17.4 (5.6)	4.6 (3.0)	4.9 (1.2)
C uptake (μmol L^{-1} d^{-1})	0.06 (0.01)	0.05 (0.03)	0.04 (0.01)
Fe:C ratio (μmol mol^{-1})	285.4 (92.5)	99.6 (88.9)	120.6 (43.3)

[a] incubation at 80% incident irradiance; [b] extracellular Fe removed using Ti(III) EDTA-citrate

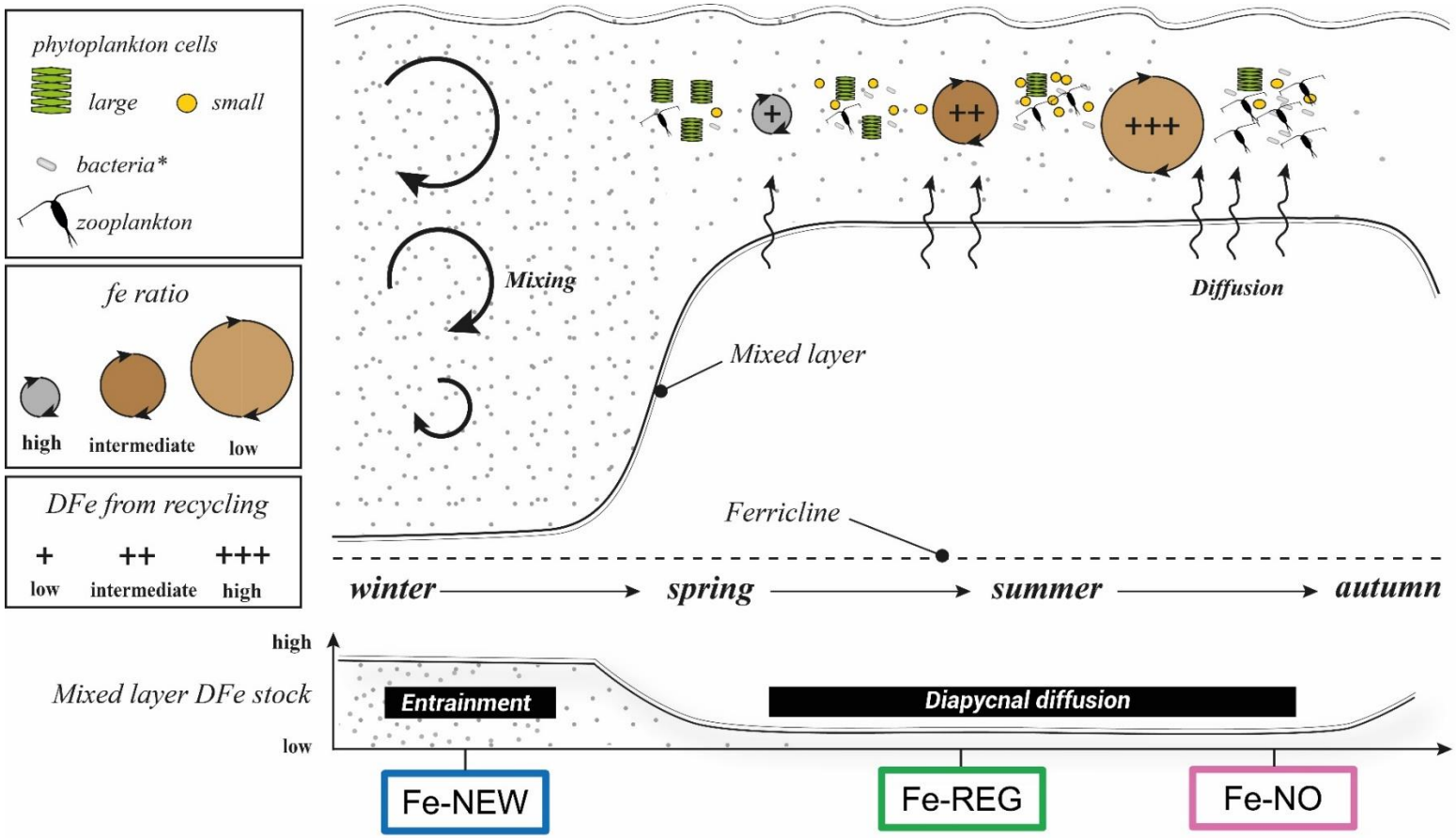

Suppl. Figure 1 A schematic representation of the seasonal variability in Southern Ocean Fe cycling adapted from Tagliabue et al. 2014. Seasonal changes in the physical supply of DFe (black arrows), mixed-layer depth and the mixed-layer DFe inventory are emphasized. The magnitude of recycling and changes in *f*e ratio are presented together (circles and cross) as well as a simplified view of the pelagic community composition. The dominant physical processes over the season is conceptualized at the bottom of the figure with the evolution of DFe inventories in the mixed layer. DFe sources (Fe-NEW, Fe-REG, and Fe-NO) used in this study aim to represent the seasonal transition of modes of DFe supply from mainly new DFe early in the season (entrainment) to regenerated DFe from recycle of sinking materials later during the summer (diapycnal diffusion) and no DFe supply.

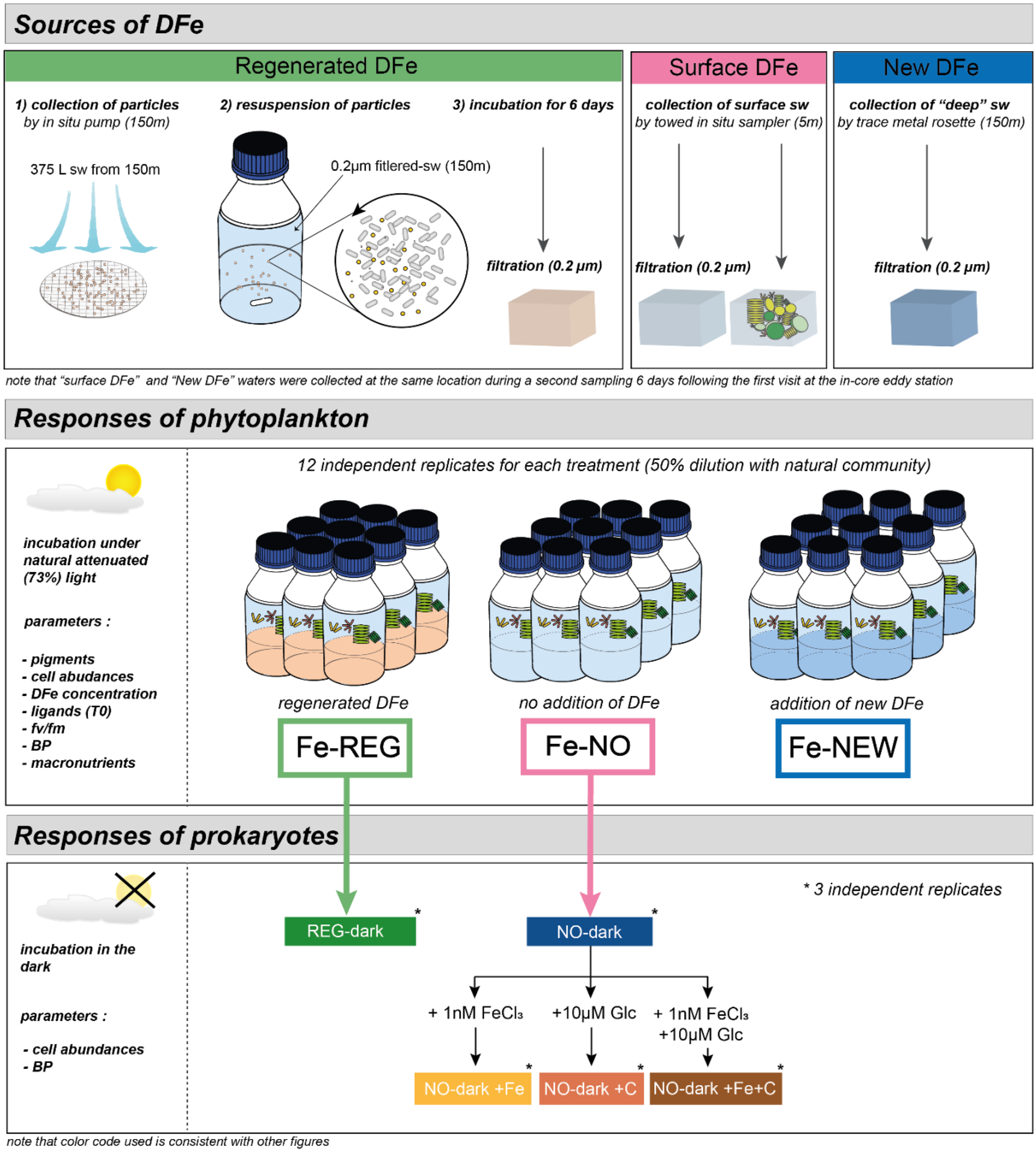

Suppl. Figure 2. A schematic representation of the experimental set-up.

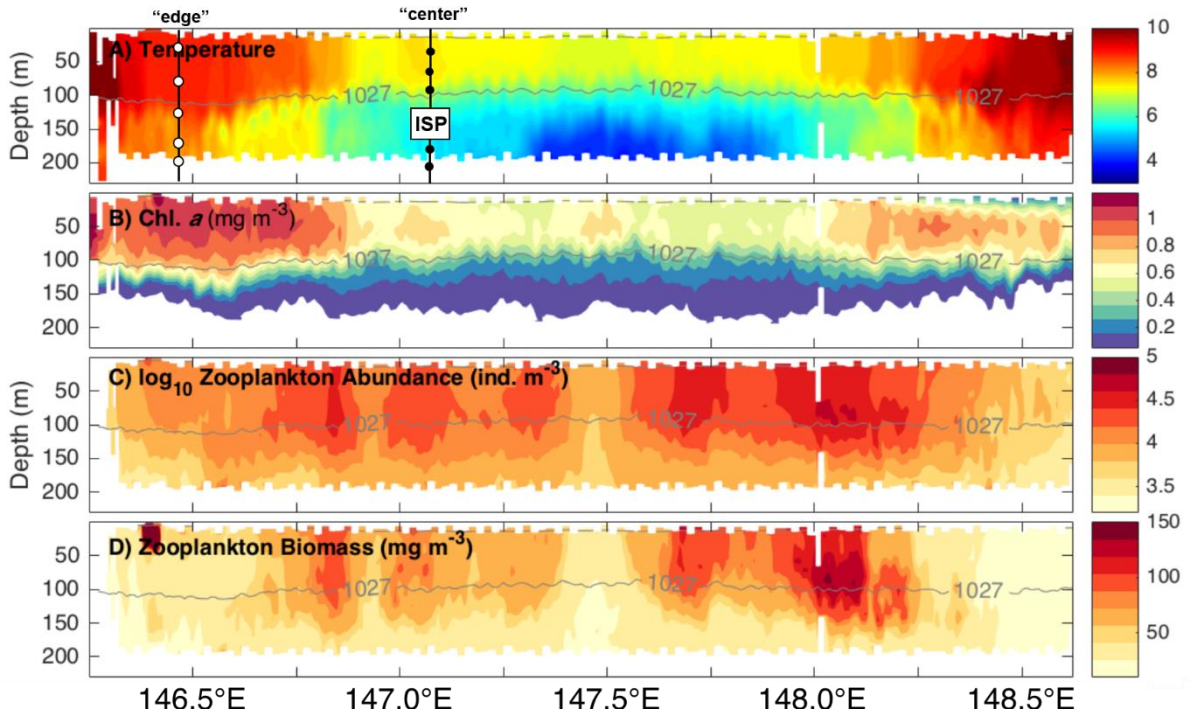

Suppl. Figure 3 (**a**) Temperature, (**b**) Chl a concentration, and zooplankton (**c**) abundance and (**d**) biomass (obtained from a Laser Optical Plankton Recorder) within the cold-core eddy and at the eddy's periphery. Location of the sampling for bacterial production profiles at the periphery ("edge", white dots) and at the within the eddy ("center", black dots) are shown in (a) panel. Sampling for surface (5m) microbial community was done at same location within the eddy ("center") as the collection of subsurface particles by In Situ Pump (ISP) deployed at 150m depth.

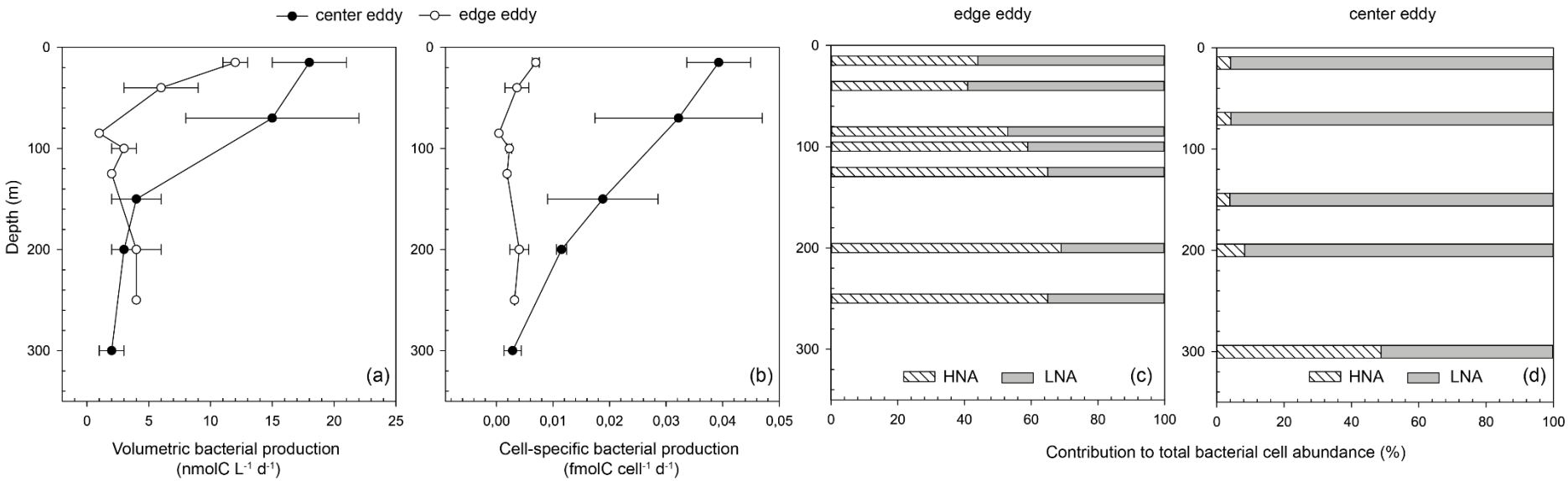

Suppl. Figure 4 Depth profiles of bacterial production and abundance at the center and at the edge of the eddy. Profiles of volumetric **(a)** and cell-specific (relative to cell abundance) bacterial production **(b)** versus depth. Error bars represent 1 standard deviation for replicate measurements. Percent of relative contribution of high DNA content (HNA) and low DNA content (LNA) cells to total bacterial abundance at the edge **(c)** and center **(d)** of the eddy.

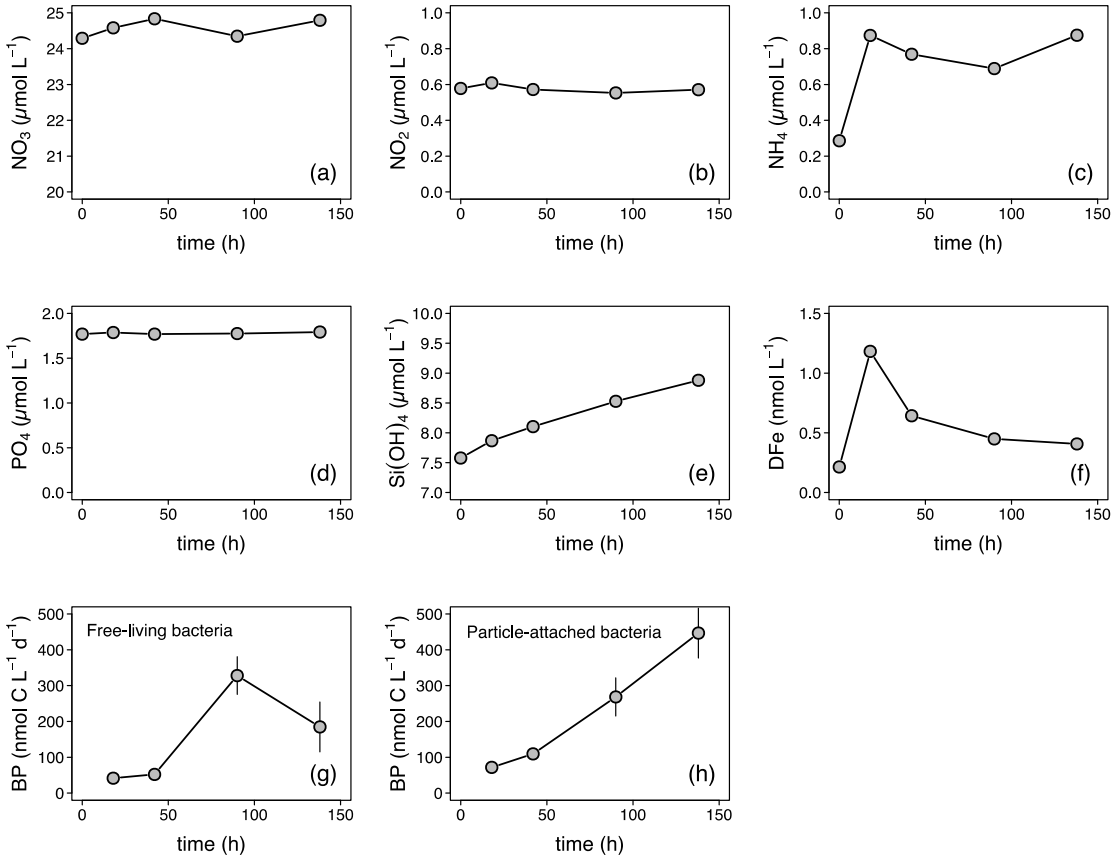

Suppl. Figure 5. Time evolution of dissolved (**a**) nitrate, (**b**) nitrite, (**c**) ammonium, (**d**) phosphate, (**e**) silicate, and (**f**) iron concentrations, and production by (**g**) free-living and (**h**) particle-attached heterotrophic bacteria during the remineralization of subsurface particles (section 2.1). Particle-attached BP was obtained by subtracting the free-living (<1-µm) from the total (unfiltered) BP.

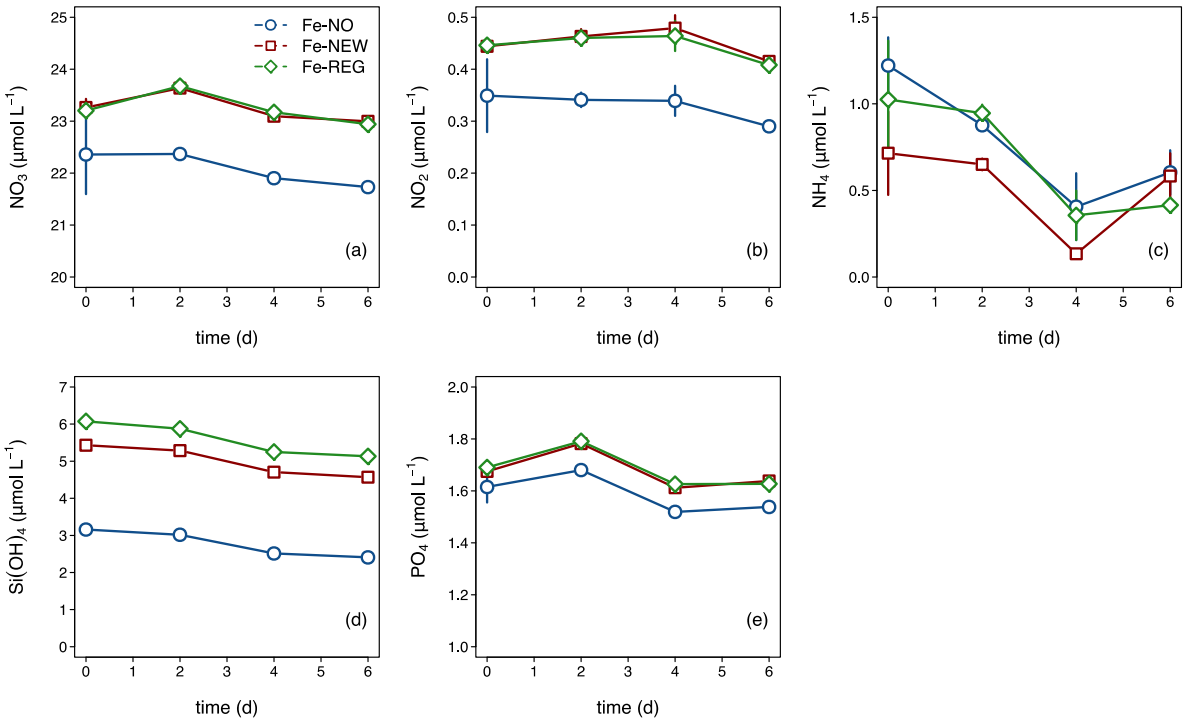

Suppl. Figure 7. Time evolution of dissolved inorganic (**a**) nitrate, (**b**) nitrite, (**c**) ammonium, (**d**) silicate, and (**e**) phosphate concentrations during the incubation. Error bars represent the standard deviation of three incubation bottle replicates.